Nano Energy 120 (2024) 109068

Contents lists available at ScienceDirect

Nano Energy

journal homepage: www.elsevier.com/locate/nanoen

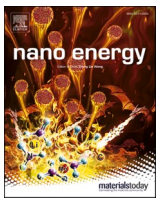

A transparent and degradable bacterial cellulose-based film for triboelectric nanogenerator: Efficient biomechanical energy harvesting and human health monitoring☆

Linan Feng [a,b], Xia Cao [b,d,e,f,g,*], Zhong Lin Wang [a,b,c,**], Liqun Zhang [a,***]

[a] Beijing University of Chemical Technology, North Third Ring Road 15, Chaoyang District, Beijing 100029, China
[b] Beijing Institute of Nanoenergy and Nanosystems, Chinese Academy of Sciences, Beijing 101400, China
[c] School of Materials Science and Engineering, Georgia Institute of Technology, Atlanta, GA 30332-0245, United States
[d] Research Center for Bioengineering and Sensing Technology, Beijing Key Laboratory for Bioengineering and Sensing Technology, School of Chemistry and Biological Engineering, and Beijing Municipal Key Laboratory of New Energy Materials and Technologies, University of Science and Technology Beijing, Beijing 100083, China
[e] Research Centre of Information Technology, Shenzhen Institute of Information Technology, Shenzhen 518172, China
[f] Shenzhen Institute for Advanced Study, University of Electronic Science and Technology of China, Shenzhen 518000, China
[g] Center on Nanoenergy Research, School of Physical Science & Technology, Guangxi University, Nanning 530004, China

ARTICLE INFO

Keywords:
Bacterial cellulose
Triboelectric nanogenerator
Energy harvesting
Signal control
Degradability
Biomechanical monitoring

ABSTRACT

In this paper, an eco-friendly and biodegradable triboelectric nanogenerator (SBB-TENG) is proposed based on bacterial cellulose (BC), sodium alginate (SA) with the introduction of barium titanate (BTO) nanoparticles. While all the composite membranes can be fully decomposed by cellulase solution within 7 h, the electrical properties of SBB-TENG are significantly improved due to the synergistic effect of enhanced dielectric constant and surface roughness of the composite membrane. Compared with SA/BC-based TENG (SBC-TENG), the voltage and current of SBB-TENGs are increased by 174 % and 193 %, respectively. In addition, the as-designed SBB TENGs are capable of serving as sensors for biomechanical monitoring, touch sensing and signal control, which greatly contributes to the development of high-performance, green and low-cost TENGs on the base of natural biodegradable materials.

1. Introduction

As an innovative energy harvesting technology that was invented by Wang et al. in 2012, triboelectric nanogenerator [1,2] (TENG) can provide sustainable power source for long-term operation of wearable/portable smart electronic devices [1–4], it can also help fullfilling [5] the rising demand for carbon neutrality [6], by harvesting low-frequency mechanical energy from the surrounding environment and convert them into electricity. In this trend, environment-friendly and biodegradable [7] TENGs that are based on green materials [8,9] (e.g., protein, rice flour, chitosan, potato starch, cellulose) could be more in line with the demand to green and renewable energy [10].

Alginate [8,11,12] is an important marine biological resource that has been widely used in medical dressings, food processing and drug carriers due to its non-toxicity, biodegradability, abundance, low cost, etc. By co-mixing with natural polysaccharides such as sodium alginate and thus introducing electron-absorbing groups, a series of cellulose-based composite membranes with different polarities can be prepared, which is expected to greatly improve the electrical properties of TENGs. Cellulose, produced by bacteria [13,14] (e.g., bacterial cellulose, BC), is an abundant natural polymer and has a three-dimensional network structure consisting of nanofibers [15,16]. The three-dimensional structure endows BC with excellent mechanical properties, good biocompatibility, biodegradability [7,17], high

☆ Professor Xia Cao, the corresponding author on this paper is the current Associate Editor of Nano Energy and Professor Z L Wang, an author on this paper is the Editor-in-Chief of Nano Energy but both have no involvement in the peer review process used to assess this work submitted to Nano Energy. This paper was assessed, and the corresponding peer review managed by Professor Chenguo Hu, also an Associate Editor in Nano Energy.

* Corresponding author at: Beijing Institute of Nanoenergy and Nanosystems, Chinese Academy of Sciences, Beijing 101400, China.
** Corresponding author at: Beijing University of Chemical Technology, North Third Ring Road 15, Chaoyang District, Beijing 100029, China.
*** Corresponding author.
E-mail addresses: caoxia@binn.cas.cn (X. Cao), zlwang@gatech.edu (Z.L. Wang), zhanglq@mail.buct.edu.cn (L. Zhang).

https://doi.org/10.1016/j.nanoen.2023.109068
Received 24 September 2023; Received in revised form 25 October 2023; Accepted 2 November 2023
Available online 12 November 2023
2211-2855/© 2023 Published by Elsevier Ltd.

porosity and high purity. More importantly, the widely distributed -OH groups and porous network structure in BC can be easily modified chemically/physically [18,19], thus serving as a workable material base for the development of TENG-based wearable energy harvesting devices and self-powered sensing systems with natural degradability, recyclability and biocompatibility [13]. For example, Zhong et al. [10]. prepared BC and chitosan (CS) semi-interpenetrating network (semi-IPN) hydrogels, the hydrogel has flexibility, high thermal stability and high mechanical properties. Zhang et al. [12]. fabricated cellulose II aerogel-based TENG, the prepared cellulose II aerogel has an interconnected open-pore three-dimensional network structure, high flexibility, high porosity, and a high surface area of 221.3 m^2g^{-1}. Yu et al. [17]. used a simple and effective method to improve bacteria cellulose (BC) based TENG, combining the enhanced dielectric constant and the

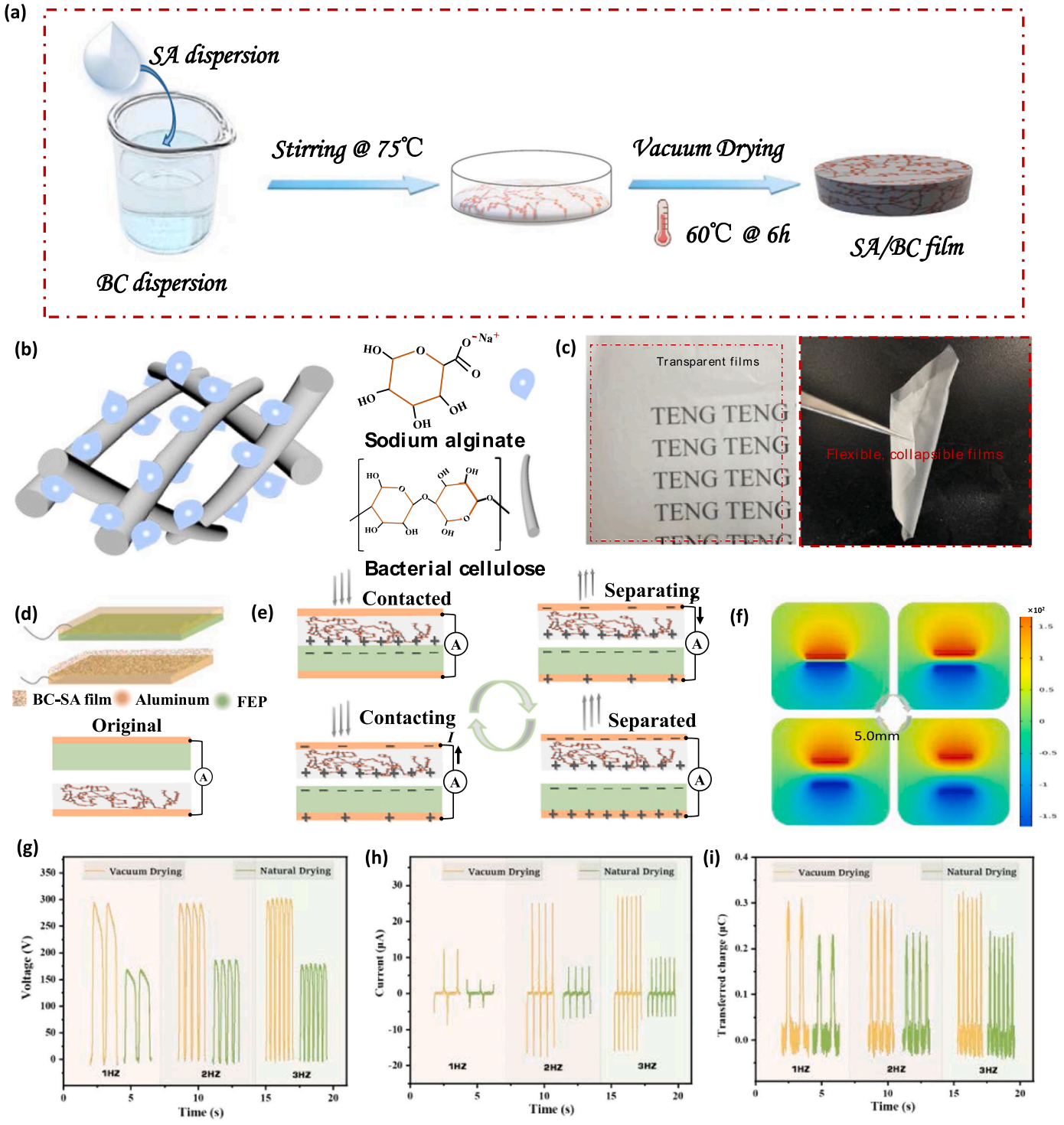

Fig. 1. (a) Schematic illustration of the preparation procedure of flexible SA/BC films. (b) Molecular structure formula of sodium alginate and bacterial cellulose. (c) The physical images of SA/BC composite films. (d)The schematic structure of TENG based on SA/BC composite films. (e)Diagram of triboelectric power generation process of SA/BC composite films. (f)Schematic diagram of the simulated evolution of the electrostatic field during TENG operation. The effect of drying conditions of SA/BC films over the output performance of SBC-TENG: (g)voltage, (h)current, (i) transferred charge.

improved surface structure of the BC composite film, the TENG has a short-circuit current of 7.1 μA, an open-circuit voltage of 87 V, and a transferred charge of 35 nC at a frequency of 3 Hz. A wide range of cellulose nanocrystal-based TENGs [12,14] as well as cellulose nanofiber-based TENGs have been reported previously, which are usually brittle and less flexible, with weaker physical strength and poorer biodegradability, which may greatly contribute to affecting the preparation and performance of TENGs.

In this study, an environmentally friendly SBC-TENG is proposed of bio degradable BC, based on which BTO nanoparticles [20,21] with high dielectric constant and low dielectric loss are incorporated for performance optimization. Due to the interaction between the BC nanofibers with high specific surface area and BTO nanoparticles, the BTO particles are uniformly dispersed and completely encapsulated in the BC nanofibers, forming a uniform and contiguous three-dimensional cellulose--based network structure. The as-designed SBB-TENGs have good mechanical response sensitivity and relatively high electrical output, with a short-circuit current, open-circuit voltage, and transmitted charge of 0.62 μA/cm^2. 530.1 V, and 350.2 nC, respectively. In addition, it takes only 60 s for the as-designed TENG to bring 47 μF@ 2.6 V by finger tapping, which is able to effectively lights potable electronics such as watch, calculator, hygrometer. The output of the SBB-TENG is significantly different when monitoring various movements. For example, the current can be generated up to 8.1μA or 15.3μA during normal mouse clicks and during high intensity operation, respectively, or during walking and running s, the output voltage is also significantly different, 101.3 V and 114.1 V, respectively. The output of SBB-TENG is significantly different when monitoring various sports, showing good sensing performance and having great application in human fatigue level, athletes' training, and patients' physical rehabilitation. Considering that all the composite membranes can be completely decomposed by cellulase solution within 7 h, this work significantly contributes to the application of natural biomaterials in high-performance, green and low-cost TENGs and other green miniature electronic sensor devices.

2. Results and discussion

Fig. 1a shows the schematic preparation of the SA/BC films by a vacuum drying method that is very convenient and eco-friendly because the whole forming procedure of SA/BC films functions without vaporized organic solution or high temperature. Fig. 1b displays the schematic chemical structure of bacterial cellulose (BC) and sodium alginate (SA), where these two components are dynamically interacting through hydrogen bonding, which is later confirmed by FTIR analysis. The physical photographs in Fig. 1c shows the transparency and flexibility of the SA/BC composite films.

The SBC-TENG in this work consists of two triboelectric layers and two electrodes. The SA/BC composite films are directly used as the positive triboelectric layer of the SBC-TENG, while the FEP films and the aluminum foils are used as the negative triboelectric layer and the top electrode respectively according to the vertical contact separation mode, as shown in Fig. 1d. The structure and working mechanism of the SBC-TENG adopting this mode are shown in Fig. 1e. In the initial state, the triboelectric material is not yet in contact and there is no transfer of charge between the two electrodes. Subsequently, the SA/BC films and FEP films are pressed into contact with each other under the action of an external force, where electrons are injected from the SA/BC films into the FEP films due to their different ability to attract electrons, resulting in positive charges on the SA/BC films surface and negative charges on the FEP films. Here, the surfaces of two films are filled with the same amount of tribological charge and are in electrical equilibrium, with no current flow or potential. The opposite charges on the surface are no longer in equilibrium when the tribological layer is gradually separating. Owing to electrostatic induction, the positive charges on the surface of the SA/BC films and the negative charges on the FEP films induce opposite induced charges at the AL electrodes, respectively, and an induced potential difference is formed between the two electrodes, driving the transfer of free electrons from the FEP electrodes to the SA/BC electrodes, generating a current in the process. The two tribological layers are in electrostatic equilibrium when they are completely separated to the maximum gap distance. Subsequently, these two tribological layers approach again, causing electrons to move in opposite ways, creating a reverse current signal. Electrons continue to flow until SA/BC is again in full contact with FEP to obtain a new electrostatic equilibrium. In this way, the two frictional electric layers are in continuous contact, and the output electric signal is generated periodically. Thus, the output of the SBC-TENG provides an AC electrical pulse signal during this periodic contact and separation process, thereby generating an electrical output to the outside. A theoretical study of the SBC-TNEG with vertical contact separation is carried out. The COMSOL Multiphysics simulation data shows the potential distribution between the upper and lower electrodes with different gaps, as shown in Fig. 1 f.

The output performance of SBC-TENG with different drying conditions of SA/BC films and different frequencies are characterized, as shown in Fig. 1g-i. The results show that the output performance of SBC-TENG assembled with the SA/BC films with vacuum drying is better than that of SBC-TENG assembled with the SA/BC films with natural drying (Fig. 1g-i). Some studies [10,12] have shown a broadening of the -OH peak in films under vacuum drying, suggesting that -OH association increases with vacuum drying, which requires more energy to destroy the -OH and therefore increases the dielectric constant, thus increasing the output performance of TENG.

The dependence of the various friction materials of SBC-TENG with an excitation frequency of 3 Hz on the current and transferred charge is further investigated. The results are shown in Fig. 2a-b. The transferred charges, short-circuit currents of SBC-TENG fabricated in polyvinyl chloride (PVC), polytetrafluoroethylene (PTFE), polyethylene terephthalate (PET), polyimide (Kapton), and fluorinated ethylene propylene (FEP) are 0.14, 0.083, 0.03, 0.14, and 0.31 μC, 8.7, 9.8, 3.7 16.4, and 26.7 μA, respectively. Obviously, higher output performance is achieved by using FEP films as another friction layer. The output performance of SBC-TENG based on different SA content at different frequencies is investigated by using FEP film as negative layer of friction. Fig. 2c-d graphically depicts that adding a certain amount of SA leads to improved output performance, and the SA/BC films with different SA contents present various voltages and currents at different frequencies, and the voltages and currents of the samples present a trend of first increase and then decrease along with the increase of SA contents. The SA/BC films with a SA content of 16.7 wt% shows the highest voltage of 302.9 V compared to other samples. This phenomenon can be explained as follows. A moderate amount of SA can increase the roughness of the SA/BC film surface [13], thus increasing the contact area of the two friction layers. In contrast, the agglomeration caused by an excessive amount of SA reduces its effect on improving the output performance. The same trend is observed for the current, with the maximum current reaching 27 μA when the SA content is 16.7 wt%.

In practical applications, the electrical output performance of the TENG under external load is of great importance. Therefore, the effective output power of the SBC-TENG (composite films containing 16.7 % SA) at different external loads (0 Ω-100 MΩ) is further investigated (Fig. 4e). The voltage tends to increase gradually as the load resistance increased, while the current tends to be reversed. The peak output voltage is up to about 313.5 V at an external load resistance of 100 MΩ. The output power (P) under different load resistance is calculated according to the formula $P = U \times I$. The results display that the output power of the SBC-TENG first increases and then decreases as the load resistance increased, ultimately the maximum instantaneous power was 1.81 mW at a load resistance of about 10 MΩ.

Fig. 2 f investigates the effect of capacitance (3.3–47μF) and drying conditions of the films (vacuum drying, natural drying) on the charging performance of the SBC-TENG. It is shown that the voltage of the charging capacitor increases with the increasing of the charging time.

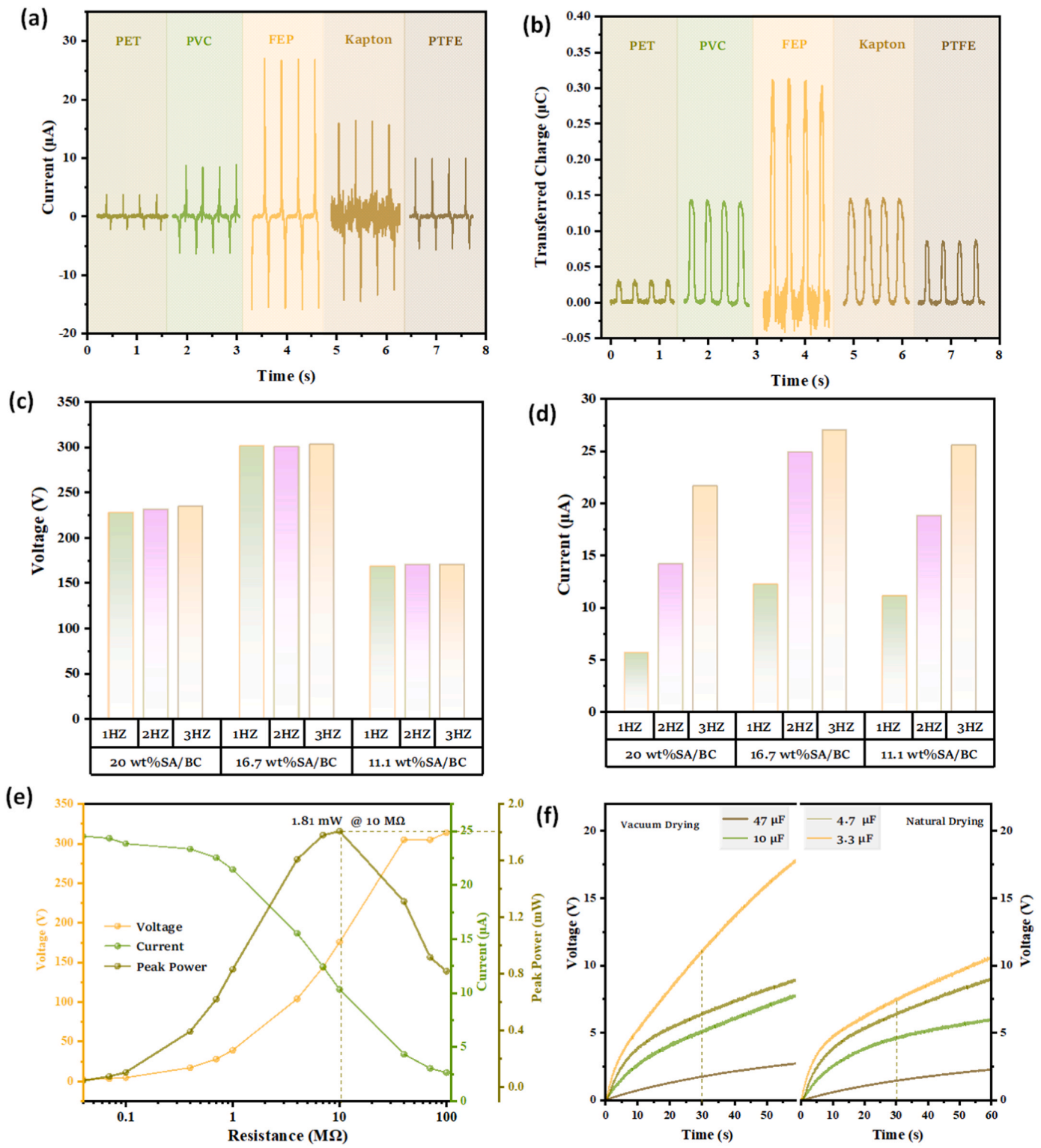

Fig. 2. The influence of five triboelectric materials on the output performance of SBC-TENG: Current(a), Transferred charge(b). Output voltage(c) and current(d) of SA/BC composite films with different sodium alginate contents at different frequencies. (e) Output voltage, current and power at different external load resistance conditions. (f) Charging capability of the SBC-TENG using capacitors with different capacitance values (3.3–47 μF).

Overall, the charging capacity of SBC-TENG assembled by SA/BC films with vacuum drying is significantly superior to that of SBC-TENG assembled by SA/BC films with natural drying. A 3.3 μF capacitor can be charged to 17.8 V in 60 s. In comparison, a 4.7 μF, 10 μF and 47 μF capacitor is able to reach 8.9 V, 7.8 V and 2.7 V at the same time.

The microscopic morphology of the surface of the prepared films is investigated using SEM, as shown in Fig. 3a-c. Fig. (3a, b, c) show the surface-section images for 11.1 wt%SA/BC films, 16.7 wt%SA/BC films, and 20 wt%SA/BC films at various magnifications. It is apparent from these figures that there are a large number of nanofibers on the surface of all BC composite membranes, which are tightly wound with each other to form a relatively flat and dense membrane, presenting a stable

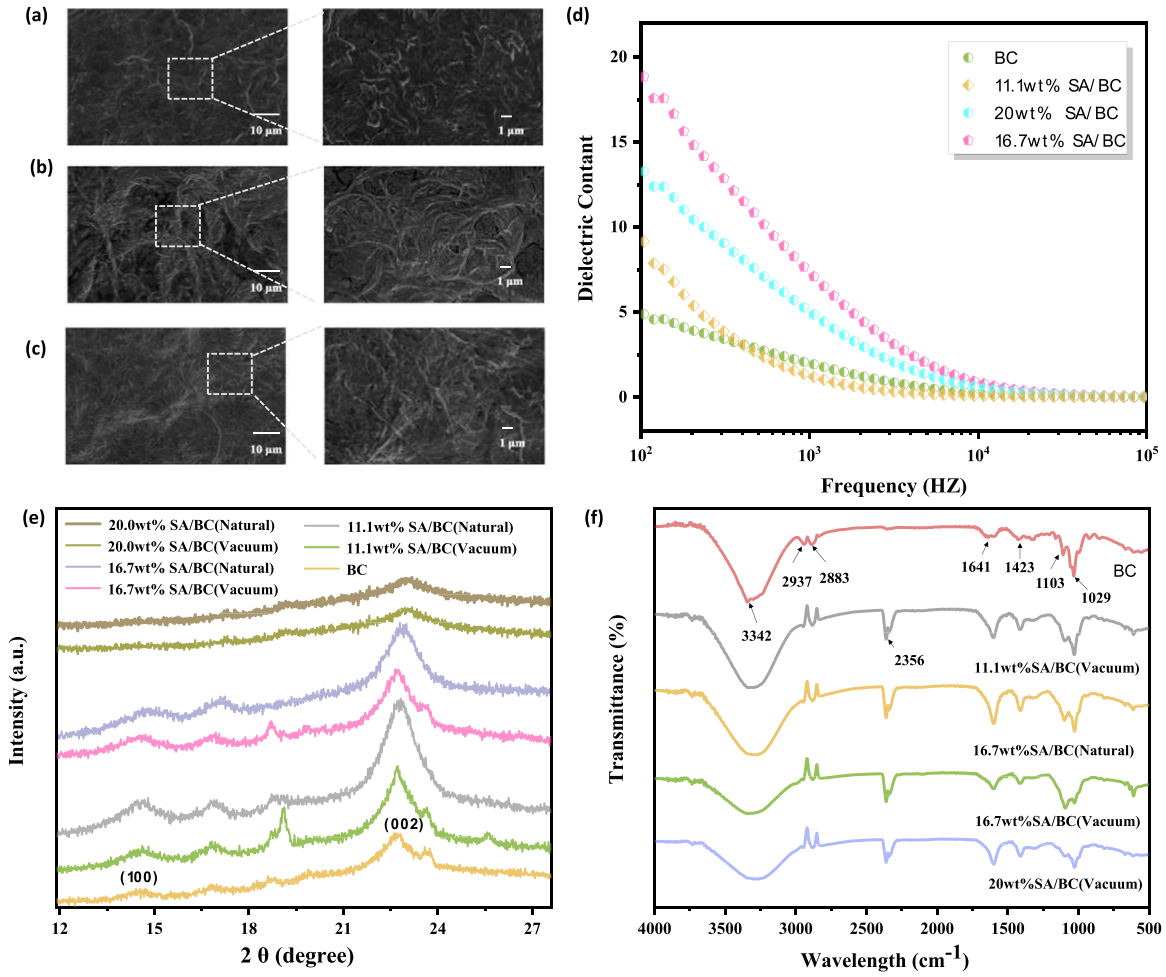

Fig. 3. Surface morphology SEM images of BC composite film, (a) 11.1 wt%SA/BC films, (b) 16.7 wt%SA/BC films, (c) 20 wt%SA/BC films. (d) Dielectric constant values of BC composite membranes with different SA contents. (e) XRD patterns and (f) FTIR spectra of pure BC, SA/BC membranes.

porous three-dimensional structure. The surface of the films become rough to different degrees when the content of SA increases (Figures S1a, b and c), showing a layered surface morphology. The transfer charge density [22] also plays a critical role in the output performance of the TENG. Increasing the dielectric constant of friction materials is an essential path to increase the charge density. Herein, sodium alginate is introduced into the BC matrix, and the dielectric properties of SA/BC composite membranes with different mass ratios of SA is compared. Fig. 3d exhibits the dielectric constant of SA/BC composite films as a function of SA content. The introduction of a certain amount of SA leads to an improvement in the dielectric constant of the SA/BC composite films compared to the pure BC films over the whole measurement frequency range. According to Equation (1) [20]:

$$\sigma_1 = \frac{d_{gap}\sigma_0}{d/\varepsilon + d_{gap}} \quad (1)$$

In which ε is dielectric constant, the enhancement of the dielectric constant boosts the output performance of TENG.

XRD patterns of pure BC films and SA/BC composite films are shown in Fig. 3e. The BC films present two broad peaks [11] at around 2θ = 14.5∘and 22.7∘, corresponding to the (1 0 0) and (002) sides of the BC. There are diffraction peaks of BC shown in the composite films, indicating the successful incorporation of BC and SA.

To verify the changes of chemical bonding on the surface, the prepared SA/BC composite films (vacuum dried, naturally dried) are characterized first by Fourier transform infrared spectroscopy (FTIR), as shown in Fig. 3 f. The peaks of pure BC membranes located at ~3342 cm^{-1}, ~2937 cm^{-1} and ~2883 cm^{-1} are attributed to the O-H stretching vibration [23,24], C-H asymmetric stretching vibration and C-H symmetric stretching vibration. The peaks at 1641 cm^{-1} and 1029 cm^{-1} are the deformation vibrations of O-H and C-O, respectively. After the addition of SA, a new peak appeared at 2356 cm^{-1}, which is the O-H vibrational peak caused by the hydrogen bonding formed by the interaction between SA and BC and the conjoining occurred, further confirming the successful doping of SA. The shift of the peaks of the stretching and deformation vibrations of O-H to lower wave numbers is probably caused by the formation of hydrogen bonds in the SA/BC composite membranes.

The preparation procedure of SA/BC/BTO composites is illustrated in Fig. 4a. The membranes are obtained by adding $BaTiO_3$ to the mixed solution of SA/BC with a vacuum drying process. The microscopic morphology of the surface of the fabricated SA/BC/BTO membranes is investigated using scanning electron microscopy, as shown in Fig. 4b. From these images, the SA/BC/BTO composite film forms a stable layer structure. The surfaces of films form a "flower bone" structure with significantly increased roughness when BTO particles are incorporated, and show a layered surface morphology. Interestingly, the BTO particles are well encapsulated in the substrate by BC, which avoids the exposure of particles. The surface of the film sample without the addition of BTO particles consists of many nanofibers, and these fibers are closely connected to each other to form a relatively flat film, and the root mean square roughness (RMS) of the pure BC film is about 16.8 nm (Fig. 4c). The roughness of SA/BC/BTO films increased due to the introduction of dielectric particles, into which, the RMS of SA/BC/BTO films increased

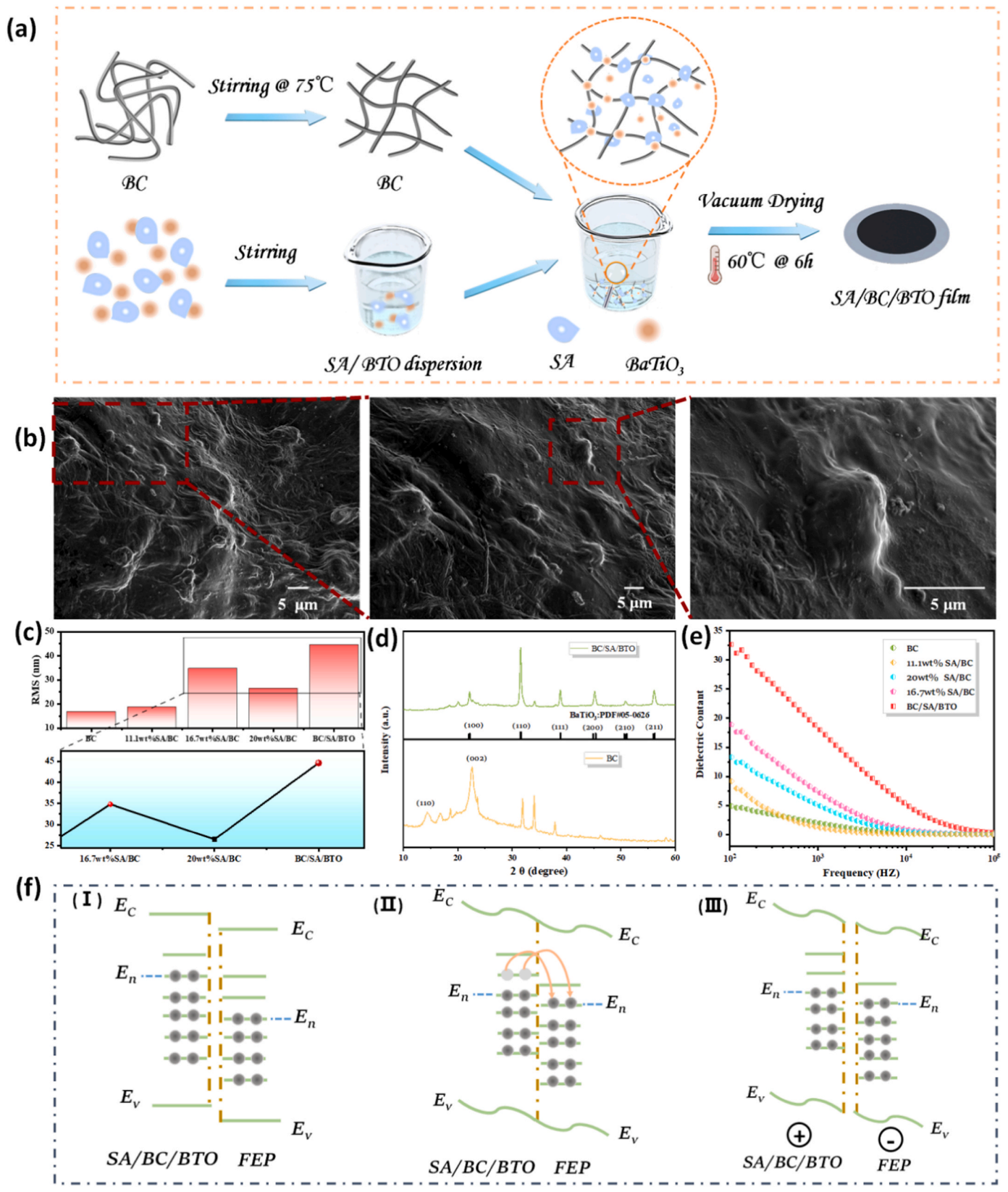

Fig. 4. (a) Schematic illustration of the preparation procedure of flexible SA/BC/BTO films. (b) The SEM images of the surface of the SA/BC/BTO films at various magnifications. (c) RMS histogram of BC composite films AFM measurements. (d) XRD patterns of pure BC, SA/BC/BTO membranes. (e) Dielectric constant values of BC composite membranes and SA/BC/BTO membranes. (f) Schematic illustration of the contact electrification mechanism between the SA/BC/BTO membrane and FEP.

to 44.6 nm, which is far superior to that of pure BC films, SA/BC composite films (e.g., 11.1 wt% SA/BC, 16.7 wt% SA/BC, 20 wt% SA/BC composite films with roughness of 18.8 nm, 34.8 nm, 26.5 nm).

The XRD image of pure BC, SA/BC/BTO films is shown in Fig. 4d. The diffraction peaks observed at 22.2, 31.6, 38.8and 45.2° are in good agreement with the crystal face of the (100), (110), (111) and (200) of $BaTiO_3$ (JCPDS #05–0626), respectively, which indicates the presence of $BaTiO_3$. The XRD peak split at $2\theta = 45.2°$indicate that $BaTiO_3$ has a tetragonal phase, suggesting that it had good ferroelectricity [21]. The pure BC films exhibit a typical diffraction peak at $2\theta = 14.4$, 18.7, 22.7, 31.9and 34.1°. The SA/BC/BTO composite films display the sequential diffraction peaks of BC and $BaTiO_3$, signifying the successfully integration of SA, BC and $BaTiO_3$.

Fig. 4e shows the variation of dielectric constants of SA/BC composite membrane and SA/BC/BTO composite membrane with different mass ratios of SA. The results demonstrate that the dielectric constant of SA/BC composite film increases firstly and then decreases with the increase of SA content. After doping with BTO dielectric particles, the dielectric constant of SA/BC/BTO composite film is shown to be a huge enhancement. That increase in dielectric constant is attributed to the spontaneous polarization of BTO particles with ferroelectric nature. The dielectric constant of SA/BC/BTO composite films is higher than other samples, which helps to increase the voltage of these devices.

The contact electrification (CE) of TENG originates from the transfer of electrons, and the barrier height of the surface of the friction material is the key factor affecting the occurrence of CE [22,25]. A model of surface states with modulated potential barrier heights is presented to explain the CE mechanism of SA/BC/BTO films versus FEP films (Fig. 4 f). It is noteworthy that the potential barrier height of the materials is related to their contact materials and chemical composition. The hydroxyl group in SA can react with the hydroxyl group in BC and the generated hydrogen bonding interacts, as well as the addition of the

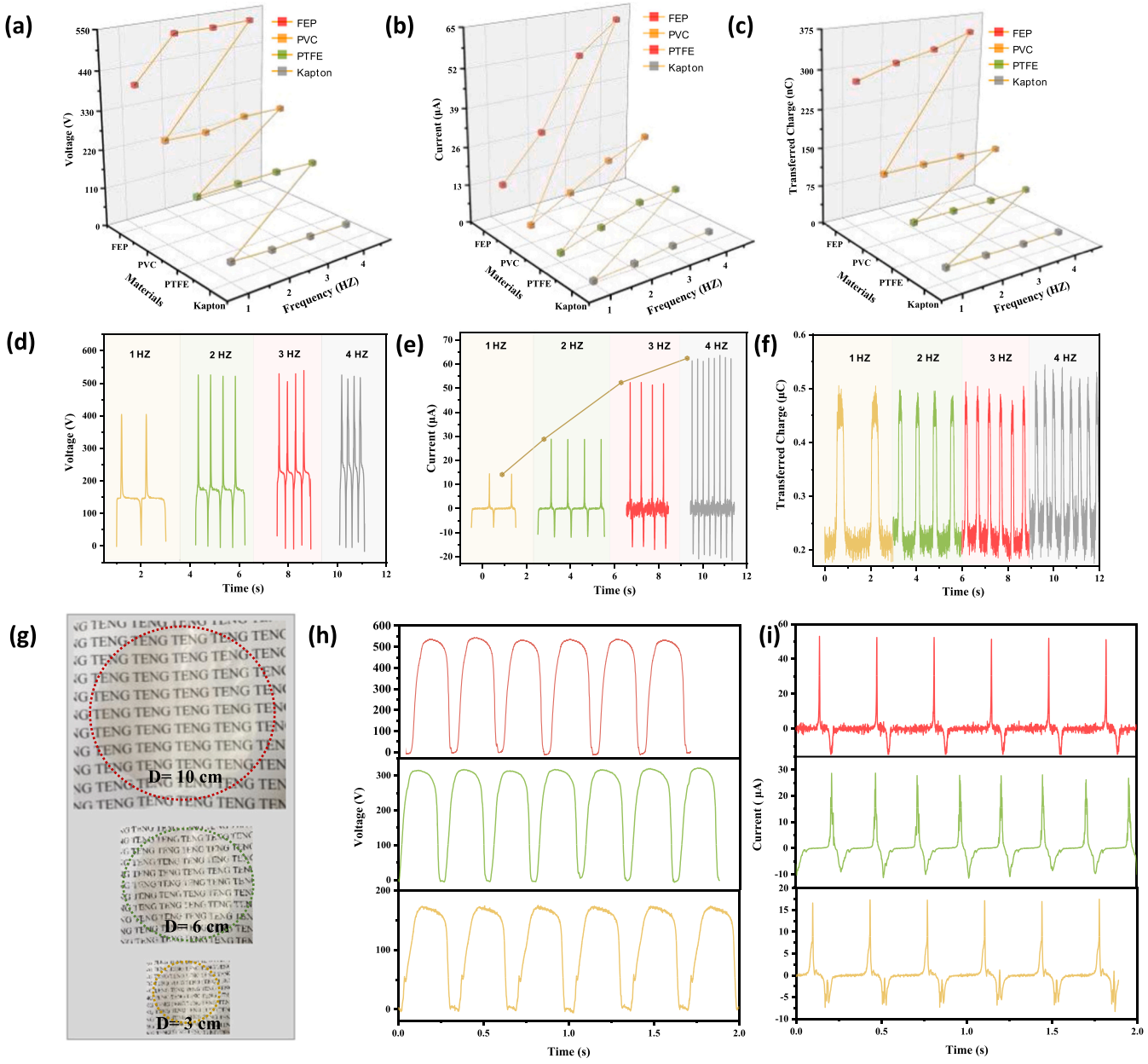

Fig. 5. Overview of (a)peak-to-peak voltages, (b) current and (c) transferred charge of the SBB-TENG under different excitations. (d) voltages, (e) currents and (f) transferred charge under different triboelectric materials with frequencies from 1 Hz to 4 Hz. (g) The physical photograph of SA/BC/BTO membranes with different diameters. The output (h)open-circuit voltage and (i) short-circuit charge of the SBB-TENG at a frequency of 3HZ, depending on the diameter of the sample.

dielectric particle $BaTiO_3$, which makes the surface state (En) of SA/BC/BTO films higher than that of FEP films. Once physical contact is generated between the SA/BC/BTO films and the FEP films, a few electrons cross the potential barrier and are transferred from the SA/BC/BTO films into the FEP films. The potential barrier decreases when the electron transfer process is completed and enters electrical equilibrium. There are positive charges on the SA/BC/BTO films and negative charges on the FEP films when the two friction layers are separated. The electrical equilibrium state is changed and electrons are driven by the potential difference through the external circuit.

Figure S2 shows the physical picture of the SBB-TENG. The output performance of SBB-TENG with different friction materials is shown in Fig. 5a-c. It is observed that the type of frictional electric material has a significant effect on the output. The FEP film exhibits the highest output performance (e.g., Q=350.2 nC, I=62.4 μA, V=530.1 V at a frequency of 4 Hz).

Fig. 5d-f shows the voltage, current and transferred charge of SBB -TENG under different contact frequencies. The output voltage of the SBB -TENG remains quite stable with only a slight increase (Fig. 5d). One possible reason for this result is that the charged state on the friction surface is not easily neutralized under high frequency conditions, leading to a large degree of electrostatic induction [5]. The current and the transferred charge increase with the increasing frequency (Fig. 5e-f). As the frequency continues to increase from 1 Hz to 4 Hz, V ranges from 406 V to 530.1 V, I ranges from 14.1 μA to 62.4 μA, and Q ranges from 284.1 nC to 350.2 nC. The electrical output of TENG is generally intuitively dependent on the physical size of the composite films. For the preparation of composite membranes, the size and shape of the membranes can be easily customized (Fig. 5 g). As can be seen from Fig. 5 h, the output voltage and current of SBB-TENGs decrease significantly when the diameter of SA/BC/BTO samples is reduced from 10 cm to 3 cm. Specifically, the SBB-TENGs with diameters of 10, 6 and 3 cm (frequency of 3 Hz) generates voltage values of 528.5, 312.5 and 173 V and current values of 52.3, 28.7 and 17.3 μA, respectively.

Energy storage devices, like capacitors, can be used to store the electrical energy obtained from the SBB-TENG for following use. During power storage, a rectifier bridge is introduced into the circuit to adjust the direction of the output current, as shown in Fig. 6a. Four capacitors of 3.3μF, 4.7μF, 10μF and 47μF are applied as accumulators. The charging curves all show a gradual increase in capacitor voltage when SBB-TENG is periodically contacted and separated (Fig. 6b). The effects of capacitance (4.7–47μF) and operating frequency (1–3 Hz) on the charging performance of the SBB-TENG have also been investigated (Fig. 6c). The data results show that capacitors with smaller capacitance or at higher operating frequencies are charged much faster. To demonstrate the high-power output of the TENG and its availability as a sustainable and clean power source for practical applications, we have evaluated the SBB-TENG as a power source by driving different external electronic devices. Some of the applications of SBB-TENG for real scenarios are demonstrated as follows. The equivalent circuit of the SBB-TENG for powering the hygrometer is shown in Fig. 6d. The capacitor is first charged by the SBB-TENG, and the charging circuit is switched to an operating circuit to connect the capacitor and the hygrometer when the voltage of the capacitor reaches 1.9 V (Fig. 6e). The hygrometer screen lights up, indicating that the hygrometer has been successfully powered up (Fig. 6 f, Video S1). In addition, the electrical energy collected and stored in the capacitor by the SBB-TENG is available to power a commercial watch (Fig. 6 g, Video S2) and a calculator (Fig. 6 h, Video S3).

Supplementary material related to this article can be found online at doi:10.1016/j.nanoen.2023.109068.

Supplementary material related to this article can be found online at doi:10.1016/j.nanoen.2023.109068.

Supplementary material related to this article can be found online at doi:10.1016/j.nanoen.2023.109068.

The photographic images of the real-time degradation of the films over 7 h are shown in Fig. 6i-k. It can see that the pure BC film, the SA/BC film and the SA/BC/BTO composite film are progressively degraded in the cellulase solution. Regarding the pure BC membranes (Fig. 6i) and the SA/BC composite membranes (Fig. 6j), the films are totally fractured in just one hour. Moreover, the size of the ruptured films gradually decreased over the next 2 h until they almost completely disappeared by the 5th hour. For SA/BC/BTO composite membranes, the degradation process becomes slower because the BTO nanoparticles and SA cover the BC substrate, making the cellulase molecules difficult to enter its interior. After 1 h, the film starts to take a curled shape and some breaks appear on the surface of the film. Starting from the 2nd hour, the SA/BC/BTO composite membranes are further degraded until they are completely depolymerized in the following 7 h.

Due to the excellent flexibility and dexterity of the BC composite film, the SBB-TENG is especially suitable for energy harvesting, motion monitoring, touch sensing and signal control because of its high sensitivity response to various mechanical stimuli, light weight, flexibility and ductility, and easy integration with heel, finger, and elbow joints. The flexible SBB-TENG is attached to the heel to collect the body's energy during walking and running. Different amplitudes and different signal styles of voltage and current outputs are obtained, as shown in Fig. 7a, b. The peak output VOC for walking and running is 101.3 and 114.1 V respectively. Such a gradual increase in voltage may be caused by an increase in the pressure exerted on the SBB-TENG as a result of the change in locomotion from walking to running.

In addition to strenuous movements, some relatively gentle movements (e.g., finger tapping, hand clapping, arm swinging) are also important biomechanical information for healthcare or human-computer interaction applications. The SBB-TENG is attached to the index finger to achieve simultaneous real-time voltage and current response to different frequencies of finger taps. Notably, the responses of voltage and current are synchronized with both low and high frequencies. During the normal mouse clicking and door knocking, the microcurrent of 8.1 μA, 4.5 μA are generated (Fig. 7d, e) In high-intensity operating conditions and emergency knocking, microcurrents of up to 15.3 μA or 8.9 μA can be generated (Fig. 7d, e). Electrical signals of different frequencies are available to remind office workers who are clicking the mouse and keyboard rapidly for long periods of time to have a proper rest. Because individuals knock on doors at different speeds, we wish to identify the characteristics of individuals knocking on doors by different characteristic electrical signal waveforms at different frequencies. In addition, the SBB-TENG can be glued to the glove (inset of Fig. 7f). Fig. 7f shows the variation of the output as a function of time when clapping the hand at different frequencies. Both the voltage and current present a stable, repeatable and recoverable signal while continuously clapping the hand. Furthermore, the SBB-TENG is affixed to the inner side of the lower arm to collect the swing arm motion energy. As the arm swings back and forth up and down, the intensity of the output signal increases and reaches a peak when the swing is completed (e.g., voltage and up to 127.6 V, 3.0 μA), as shown in Fig. 7 g. The output of SBB-TENG is significantly different as monitoring various sports and shows good sensing performance, which has potential application value in athletes' training, physical exercise and patients' physical rehabilitation.

Durability and stability are two important characteristics that affect the practical application of TENG. The long-term operating capability of the SBB-TENG is examined by testing its output current at 3HZ for over 600 cycles. Fig. 7 h displays that the current remains essentially constant after continuous operation and the output is not degraded. This implies that both the electrodes and the frictional electric material are of good durability and reliability. The output of SBB-TENG is also investigated after 2 months of standing in air to characterize the environmental stability of the SA/BC/BTO composite films, as shown in Fig. 7i. Surprisingly, the SBB-TENG still maintains good and stable output performance without degradation after being stored in air for 2 months.

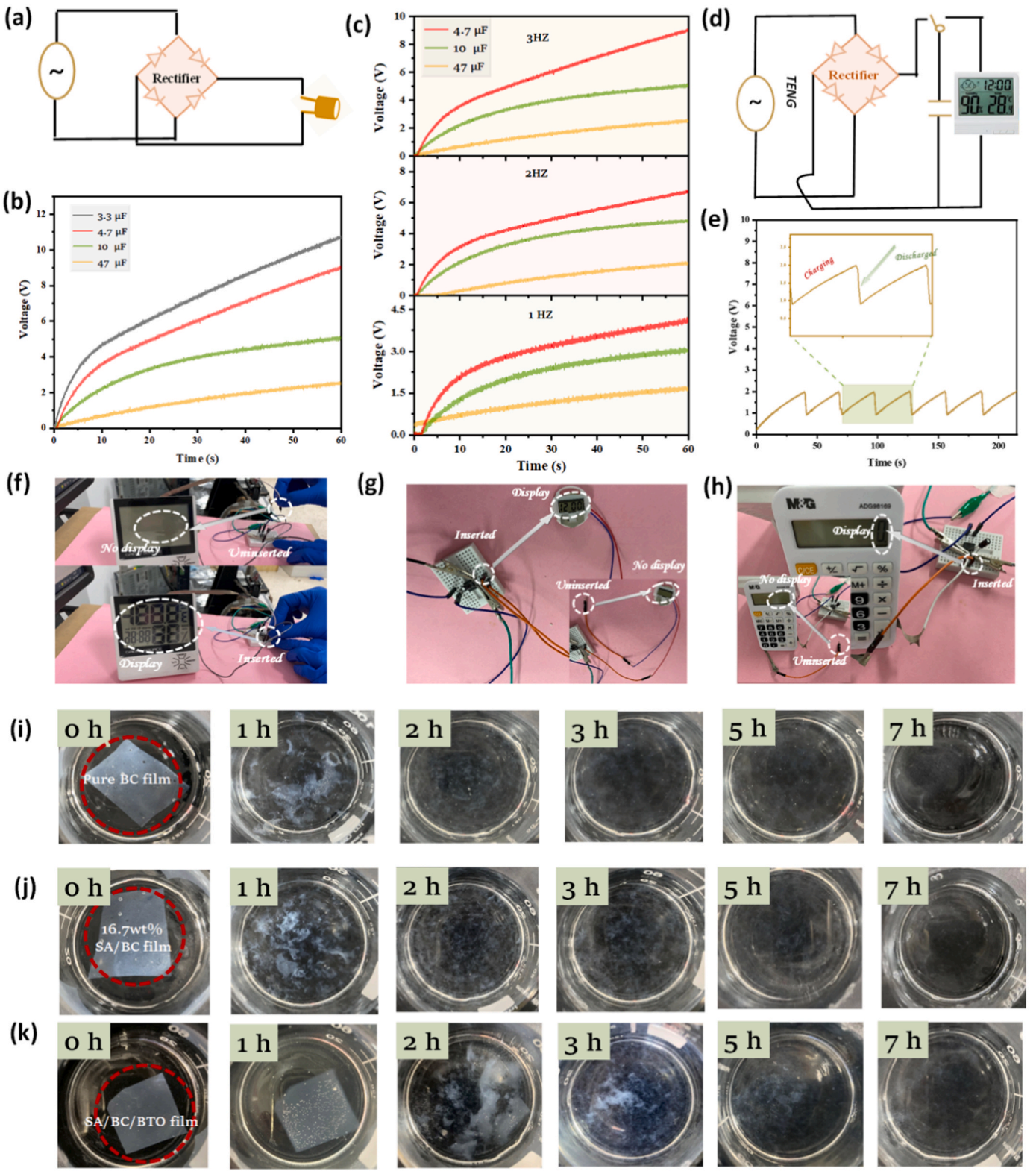

Fig. 6. (a) Circuit diagram for charging capacitors. (b) The ability to charge the SBB-TENG at a frequency of 3HZ using capacitors of different capacitance values (3.3μF-47μF). (c) Charging capability of the SBB-TENG using capacitors with different capacitance values(4.7μF-47μF) at different frequencies(1–3HZ). (d) Circuit diagram for charging a hygrometer. (e) Charging voltage profile versus charging time for powering a hygrometer. The hygrometer(f), Electronic watches(g) and (h) calculators that can be powered. Images of the degradation process of (i) pure BC films and (j) 16.7 wt% SA/BC membranes (k) SA/BC/BTO membranes in the presence of cellulase.

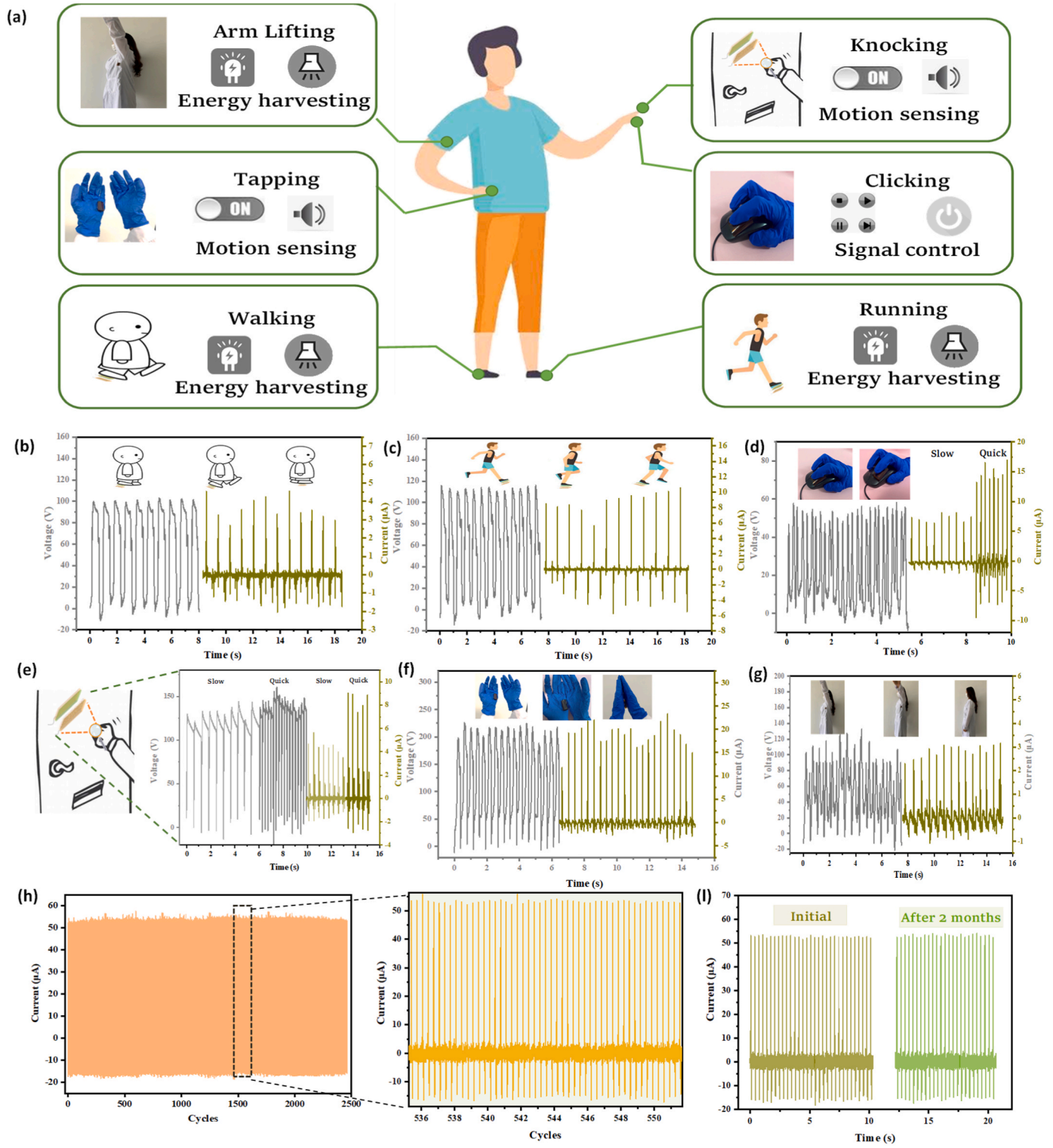

Fig. 7. (a) Illustration of wearable sensors for different parts of the body. The output voltage versus time during (b) walking, (c) running, (d) clicking the mouse, (e) knocking the door, (f) tapping, (g)lifting arm. Inset: Photographs of several movements of a person during exercise. (h) Output voltage stability of the SBB-TENG. (l) The stability of SBB-TENG in air.

3. Conclusion

We propose an eco-friendly TENGs based on BC nanofibers and SA. There is a significant improvement in the output properties of SA/BC/BTO-based TENGs after the introduction of nano-BTO particles due to the synergistic effect of the increase in dielectric constant and surface roughness of the composite films. Compared to pure SA/BC membranes, the voltage and current are increased by 174 % and 193 %, respectively. In addition, cellulose-based-TENGs show good biodegradability and excellent flexibility, which promote their application and also enhance their performance in mechanical energy harvesting, biomechanical monitoring, touch sensing and signal control. This work contributes to

the application of natural biomaterials in the field of TENGs and other electronic sensor devices.

4. Experimental section

4.1. Materials

BC membranes were supplied by LaiDe Chemical Fiber Group Ltd. (HaiNan, China). SA and BTO nanoparticles were purchased from Shanghai Maclean Biochemical Technology Co. Polyvinylidene fluoride was obtained from Shanghai Aladdin Biochemical Technology Co.

4.2. Preparation of SA/BC composites

First, the BC membranes were purified by the previously reported method. Then mechanical homogenization was performed by using a soymilk machine and a dispersion of BC nanofibers (0.1 g/ml) was obtained. A certain amount of sodium alginate (11.1 wt%,16.7 wt%,20 wt % by mass of sodium alginate) was added to the BC solution, followed by 1 g of glycerol and 0.625 g of sodium carboxymethyl cellulose, and the mixed solution was allowed to stir at 75 °C for 3 h. The BC/SA composite films were prepared by pouring the well-mixed solution inside the Petri dishes and under vacuum at 60 °C as well as natural conditions, respectively.

4.3. Preparation of SA/BC/BTO composites

SA/BC/BTO composites were prepared under the optimized SA reaction conditions. A certain amount of barium titanate and polyvinylidene fluoride was added to the SA/BC mixture and stirred at 75 °C for 3 h. The solution was then poured into Petri dishes and dried overnight at 60 °C in a vacuum oven.

4.4. Fabrication of triboelectric nanogenerator (TENG)

Circles with diameters of 10 cm, 6 cm, and 3 cm were cut from SA/BC composite film and SA/BC/BTO composite film, respectively, and then aluminum foil was pasted as the frictional electric positive layer, and aluminum foil was used as the electrode. FEP was used as the friction electronegative layer. The frictional electric positive and negative layers were arranged face-to-face with polyimide film to prepare vertical contact TENG.

4.5. Characterization and measurement

The surface morphology of SA/BC composite films and SA/BC/BTO composite films was characterized by AFM atomic force microscopy (MFP-3D-SA). Morphology of composite films was characterized by Nova Field Emission Scanning Electron Microscope (Nova Nano SEM 450). The crystal and infrared spectra of the composite films were measured by XRD powder (Xpert3 Powder) and Fourier transform infrared spectroscopy (FTIR), respectively. The TENG was connected to a linear motor, an electronic measuring instrument (Keithley 6514) and an oscilloscope were used to measure open circuit voltage, short circuit current and transferred charge.

CRediT authorship contribution statement

Linan Feng: Conceptualization, Methodology, Writing – original draft. **Xia Cao:** Data curation, Software, Supervision. **Zhong Lin Wang:** Visualization, Investigation. **Liqun Zhang:** Writing – review & editing.

Author contributions

This manuscript was written through contributions of all authors. All authors have given approval to the final version of the manuscript.

Declaration of Competing Interest

No conflict of interest exits in the submission of this manuscript. I would like to declare on behalf of my co-authors that the work described was original research that has not been published previously, and not under consideration for publication elsewhere, in whole or in part.

Data availability

Data will be made available on request.

Acknowledgements

This work was financially supported by the National Key R & D Project from Minister of Science and Technology (2021YFA1201601), and the Key Research Program of Frontier Sciences, CAS (ZDBS-LY-DQC025). Patents have been filed to protect the reported inventions.

Appendix A. Supporting information

Supplementary data associated with this article can be found in the online version at doi:10.1016/j.nanoen.2023.109068.

References

[1] H. Wu, Y. Huang, F. Xu, Y. Duan, Z. Yin, Energy harvesters for wearable and stretchable electronics: from flexibility to stretchability, Adv. Mater. 28 (45) (2016) 9881–9919.
[2] X. Cao, Y. Jie, P. Ma, Power generation by contact and the potential applications in new energy, Nano Energy 87 (2021).
[3] P. Chen, Y. Luo, R. Cheng, S. Shu, J. An, A. Berbille, T. Jiang, Z.L. Wang, Achieving high power density and durability of sliding mode triboelectric nanogenerator by double charge supplement strategy, Adv. Energy Mater. 12 (33) (2022).
[4] S.W. Chen, X. Cao, N. Wang, L. Ma, H.R. Zhu, M. Willander, Y. Jie, Z.L. Wang, An ultrathin flexible single-electrode triboelectric-nanogenerator for mechanical energy harvesting and instantaneous force sensing, Adv. Energy Mater. 7 (1) (2017).
[5] X. Cao, Y. Jie, P. Ma, Z.L. Wang, Wherever there is a dynamic touch, there is electromagnetic field——a discovery for power generation, Nano Energy 78 (2020).
[6] F. Xing, Y. Jie, X. Cao, T. Li, N. Wang, Natural triboelectric nanogenerator based on soles for harvesting low-frequency walking energy, Nano Energy 42 (2017) 138–142.
[7] X. Guo, F. Yang, X. Sun, Y. Bai, G. Liu, W. Liu, R. Wang, X. He, Anti-freezing self-adhesive self-healing degradable touch panel with ultra-stretchable performance based on transparent triboelectric nanogenerators, Adv. Funct. Mater. 32 (31) (2022).
[8] F. Wahid, X.H. Hu, L.Q. Chu, S.R. Jia, Y.Y. Xie, C. Zhong, Development of bacterial cellulose/chitosan based semi-interpenetrating hydrogels with improved mechanical and antibacterial properties, Int J. Biol. Macromol. 122 (2019) 380–387.
[9] L. Li, Z. Lin, X. Yang, Z. Wan, S. Cui, A novel cellulose hydrogel prepared from its ionic liquid solution, Sci. Bull. 54 (9) (2009) 1622–1625.
[10] F. Wu, B. Lan, Y. Cheng, Y. Zhou, G. Hossain, G. Grabher, L. Shi, R. Wang, J. Sun, A stretchable and helically structured fiber nanogenerator for multifunctional electronic textiles, Nano Energy 101 (2022).
[11] L. Zhang, Y. Liao, Y.C. Wang, S. Zhang, W. Yang, X. Pan, Z.L. Wang, Cellulose II aerogel-based triboelectric nanogenerator, Adv. Funct. Mater. 30 (28) (2020), 2001763.
[12] Y. Pang, F. Xi, J. Luo, G. Liu, T. Guo, C. Zhang, An alginate film-based degradable triboelectric nanogenerator, RSC Adv. 8 (12) (2018) 6719–6726.
[13] P. Cazón, M. Vázquez, Bacterial cellulose as a biodegradable food packaging material: a review, Food Hydrocolloid 113 (2021).
[14] H.-J. Kim, E.-C. Yim, J.-H. Kim, S.-J. Kim, J.-Y. Park, I.-K. Oh, Bacterial nanocellulose triboelectric nanogenerator, Nano Energy 33 (2017) 130–137.
[15] B. Fatma, S. Gupta, C. Chatterjee, R. Bhunia, V. Verma, A. Garg, Triboelectric generators made of mechanically robust PVDF films as self-powered autonomous sensors for wireless transmission based remote security systems, J. Mater. Chem. A 8 (30) (2020) 15023–15033.
[16] H. Yu, Y. Shao, C. Luo, Y. Li, H.-z Ma, Y.-h Zhang, B. Yin, J.-b Shen, M.-b Yang, Bacterial cellulose nanofiber triboelectric nanogenerator based on dielectric particles hybridized system, Compos. Part A Appl. Sci. Manuf. 151 (2021).
[17] M. Kang, M.S. Bin Mohammed Khusrin, Y.-J. Kim, B. Kim, B.J. Park, I. Hyun, I. M. Imani, B.-O. Choi, S.-W. Kim, Nature-derived highly tribopositive κ-carrageenan-agar composite-based fully biodegradable triboelectric nanogenerators, Nano Energy 100 (2022).

[18] J. Huang, Y. Hao, M. Zhao, H. Qiao, F. Huang, D. Li, Q. Wei, Biomass-based wearable and self-powered pressure sensor for human motion detection, Compos. Part A Appl. Sci. Manuf. 146 (2021).
[19] S. Jakmuangpak, T. Prada, W. Mongkolthanaruk, V. Harnchana, S. Pinitsoontorn, Engineering bacterial cellulose films by nanocomposite approach and surface modification for biocompatible triboelectric nanogenerator, ACS Appl. Electron. Mater. 2 (8) (2020) 2498–2506.
[20] Y. Shao, C.-p Feng, B.-w Deng, B. Yin, M.-b Yang, Facile method to enhance output performance of bacterial cellulose nanofiber based triboelectric nanogenerator by controlling micro-nano structure and dielectric constant, Nano Energy 62 (2019) 620–627.
[21] Z. Sun, L. Yang, S. Liu, J. Zhao, Z. Hu, W. Song, A green triboelectric nanogenerator composite of degradable cellulose, piezoelectric polymers of PVDF/PA6, and nanoparticles of BaTiO3, Sensors 20 (2) (2020).
[22] C. Xu, Y. Zi, A.C. Wang, H. Zou, Y. Dai, X. He, P. Wang, Y.C. Wang, P. Feng, D. Li, Z. L. Wang, On the electron-transfer mechanism in the contact-electrification effect, Adv. Mater. 30 (15) (2018), e1706790.
[23] V.K. Bharti, A.D. Pathak, C.S. Sharma, M. Khandelwal, Ultra-high-rate lithium-sulfur batteries with high sulfur loading enabled by Mn2O3-carbonized bacterial cellulose composite as a cathode host, Electrochim. Acta 422 (2022).
[24] S. Chen, Y. Chen, D. Li, Y. Xu, F. Xu, Flexible and sensitivity-adjustable pressure sensors based on carbonized bacterial nanocellulose/wood-derived cellulose nanofibril composite aerogels, ACS Appl. Mater. Interfaces 13 (7) (2021) 8754–8763.
[25] C. Xu, B. Zhang, A.C. Wang, W. Cai, Y. Zi, P. Feng, Z.L. Wang, Effects of metal work function and contact potential difference on electron thermionic emission in contact electrification, Adv. Funct. Mater. 29 (29) (2019).

Linan Feng is currently a doctoral student jointly trained by Beijing University of Chemical Technology (BUCT) and Beijing Institute of Nanoenergy and Nanosystems, Chinese Academy of Sciences. Her research interests include frictional electric nanogenerators, self-powered micro/nanosystems, and energy materials.

Xia Cao is currently a distinguished professor at the University of Science and Technology Beijing, and a professor at the Beijing Institute of Nanoenergy and Nanosystems, Chinese Academy of Sciences. Her main research interests include energy materials, nanogenerator, energy conversion and storage, flexible electronic sensor, and self-powered system.

Zhong Lin Wang received his Ph.D. from Arizona State University in physics. He now is the Hightower Chair in Materials Science and Engineering, Regents' Professor, Engineering Distinguished Professor and Director, Center for Nanostructure Characterization, at Georgia Tech. Prof. Wang has made original and innovative contributions to the synthesis, discovery, characterization and understanding of fundamental physical properties of oxide nanobelts and nanowires, as well as applications of nanowires in energy sciences, electronics, optoelectronics and biological science. His discovery and breakthroughs in developing nanogenerators established the principle and technological roadmap for harvesting mechanical energy from the environment and biological systems for powering personal electronics. His research on self-powered nanosystems has inspired the worldwide effort in academia and industry for studying energy for micro-nano-systems, which is now a distinct disciplinary in energy research and future sensor networks. He coined and pioneered the field of piezotronics and piezophototronics by introducing piezoelectric potential gated charge transport process in fabricating new electronic and optoelectronic devices. Details can be found at: www.nanoscience.gatech.edu.

Liqun Zhang is a professor of Beijing University of Chemical Technology. His research interests focus on rubber science and technology, polymer nanocomposites, bio-based polymeric materials and so on. He has received various famous awards such as National Outstanding Youth Foundation, Changjiang Scholar Professor of Ministry of Education of China, Sparks-Thomas sci-tech award of Rubber Division of American Chemical Society, Science of Chemical Engineering of Japan (SCEJ) Research award, and Morand Lambla Award of International Polymer Processing Society. He has published over 300 peer-reviewed papers, and has given over 60 plenary/keynote/invited lectures in international conferences.